

OBJECT2SCENE: PUTTING OBJECTS IN CONTEXT FOR OPEN-VOCABULARY 3D DETECTION

Chenming Zhu¹ Wenwei Zhang¹ Tai Wang¹ Xihui Liu^{2*} Kai Chen^{1*}

¹Shanghai AI Laboratory ²The University of Hong Kong

{zhuchenming, zhangwenwei, wangtai, chencai}@pjlab.org.cn
xihuiliu@eee.hku.hk

ABSTRACT

Point cloud-based open-vocabulary 3D object detection aims to detect 3D categories that do not have ground-truth annotations in the training set. It is extremely challenging because of the limited data and annotations (bounding boxes with class labels or text descriptions) of 3D scenes. Previous approaches leverage large-scale richly-annotated image datasets as a bridge between 3D and category semantics but require an extra alignment process between 2D images and 3D points, limiting the open-vocabulary ability of 3D detectors. Instead of leveraging 2D images, we propose *Object2Scene*, the first approach that leverages large-scale large-vocabulary 3D object datasets to augment existing 3D scene datasets for open-vocabulary 3D object detection. *Object2Scene* inserts objects from different sources into 3D scenes to enrich the vocabulary of 3D scene datasets and generates text descriptions for the newly inserted objects. We further introduce a framework that unifies 3D detection and visual grounding, named *L3Det*, and propose a cross-domain category-level contrastive learning approach to mitigate the domain gap between 3D objects from different datasets. Extensive experiments on existing open-vocabulary 3D object detection benchmarks show that *Object2Scene* obtains superior performance over existing methods. We further verify the effectiveness of *Object2Scene* on a new benchmark OV-ScanNet-200, by holding out all rare categories as novel categories not seen during training.

1 INTRODUCTION

Point cloud-based 3D object detection aims at localizing and recognizing objects from 3D point cloud of scenes. It is a fundamental task in 3D scene perception where remarkable progress has been made in recent years (Zhou et al., 2022b; Liu et al., 2021; Shi et al., 2020; Misra et al., 2021). However, the ability of 3D detection is limited to a small vocabulary due to the limited number of annotated categories in 3D point cloud datasets. As a critical step towards generalizing 3D object detection to real-world scenarios, open-vocabulary 3D object detection aims at detecting categories without annotations in the training set.

Mainstream open-vocabulary 2D detection methods rely on large-scale image-text datasets (Ridnik et al., 2021; Lin et al., 2023) or models pre-trained on these datasets (Gu et al., 2021; Kuo et al., 2022) to provide additional knowledge on the general representations for unseen categories. Unfortunately, similar point-text data pairs are limited due to the expenses of 3D annotations and point cloud collection, making those 2D approaches not directly applicable to the 3D scenario. Previous approaches (Lu et al., 2023; 2022) leverage richly annotated image datasets as a bridge and transfer knowledge from images to 3D point clouds to address this challenge. However, these images and point clouds typically do not have explicit correspondences, which casts a severe challenge for 2D-3D alignment and hinders the open-vocabulary ability of 3D detectors. Besides, the generated pseudo 3D bounding boxes based on 2D detectors are sub-optimal and limit the open-vocabulary 3D detection capability in the localization stage.

*Correspondence to xihuiliu@eee.hku.hk, chencai@pjlab.org.cn.

The recently proposed large-scale 3D object datasets (Chang et al., 2015; Uy et al., 2019; Deitke et al., 2022) pave the way for learning large-vocabulary 3D object representations without 2D data. These 3D object datasets have been used in recent 3D recognition methods (Zhang et al., 2022; Zhu et al., 2022; Xue et al., 2023), achieving astonishing open-vocabulary point cloud recognition ability. However, these methods can not address the issue of localizing objects required in 3D detection. Different from 2D images, a 3D object could be easily inserted into a point cloud scene accompanied by naturally precise 3D location and box annotation. Therefore, we raise the question: *can we train the models to learn open-vocabulary 3D object detection by leveraging 3D object datasets to augment 3D scene datasets?* The 3D scene datasets are foundational for 3D object detection with limited categories, while the 3D object datasets can act as a database of 3D objects to largely enrich the vocabulary size of the 3D detector.

An intuitive augmentation approach could be putting the large-scale 3D objects in the 3D context to broaden the vocabulary size. Based on the augmented context, the 3D detector can access large-vocabulary 3D objects with precise 3D location and box annotation. However, such a naive 3D object insertion approach leads to an *inconsistent annotation issue*, where the unseen category objects from the original scene are not annotated, but the unseen category objects that are newly inserted into the scene are annotated. To this end, we propose **Object2Scene**, which puts objects into the 3D context to enrich the vocabulary of 3D scene datasets and generates text prompts for the newly inserted objects. Specifically, we choose seen objects in the scene as reference objects to guide the physically reasonable 3D object insertion according to their physical affordance. Besides, to mitigate this inconsistent annotation issue, we introduce language grounding prompts to diminish the ambiguity of class label annotations. The generated grounding prompts such as “a table that is near a plant that is at the room center” could eliminate the ambiguity and refer to the specific inserted table. By such construction, we can achieve scene-level 3D object-text alignment in a large vocabulary space.

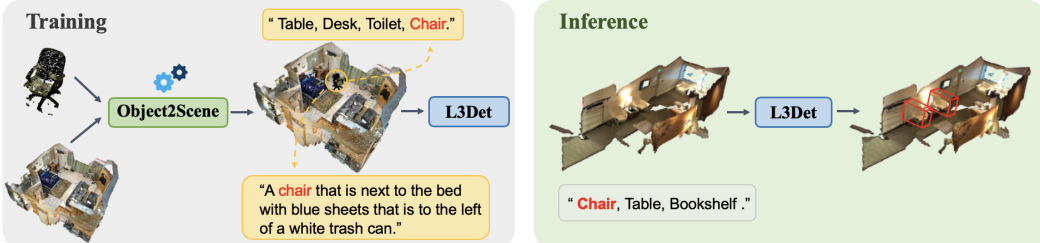


Figure 1: By utilizing the 3D object datasets, Object2Scene empowers the 3D detector (L3Det) with strong open-vocabulary capability. The training process is shown on the left, where Object2Scene generates training data for L3Det by inserting unseen objects into the 3D scene and generating grounding prompts for the inserted objects. The inference process is shown on the right.

Furthermore, we explore the model design of open-vocabulary 3D object detection with Object2Scene. To adapt the model for both object category annotations and language grounding prompts, we propose a unified model, named **Language-grounded 3D point-cloud Detection (L3Det)**, for 3D detection and 3D language grounding. L3Det takes the point cloud of a 3D scene and a text prompt (the text prompt for object detection is a list of object categories) as input, and grounds the prompt to object bounding boxes with a transformer-based encoder-decoder architecture. Since we mainly align the 3D objects from 3D object datasets with the text in the large vocabulary space, another challenge of Object2Scene is *the domain gaps between inserted objects from 3D object datasets and existing objects in the original 3D scene datasets*. We further introduce a **Cross-domain Category-level Contrastive Learning** approach to mitigate such domain gaps. Specifically, the contrastive loss specifically aims to bring feature representations of same-category objects closer together and push feature representations of different-category objects farther apart, regardless of the source datasets. The proposed cross-domain category-level contrastive learning method further reduces the domain gap between feature representations of the inserted 3D objects and the original 3D scenes, and guides the model towards learning source-agnostic generalizable 3D representations.

Our contributions are summarized as follows. 1) We propose Object2Scene, the first approach that leverages large-scale large-vocabulary 3D object datasets and existing 3D scene datasets for open-vocabulary 3D object detection, by inserting 3D objects into 3D scenes and generating language

grounding prompts for the inserted objects. 2) We introduce a language-grounded 3D detection framework L3Det to achieve 3D object-text alignment and propose a novel cross-domain category-level contrastive learning method to mitigate the domain gap between inserted 3D objects and original 3D scenes in Object2Scene. 3) We evaluate Object2Scene on open-vocabulary 3D object detection benchmarks on ScanNet and SUN RGB-D, and validate the effectiveness of our proposed approach with extensive experiments.

2 RELATED WORK

2.1 3D OBJECT DATASETS

Current 3D object datasets can be divided into two categories: synthetic and real-scanned. For the synthetic CAD model datasets, ShapeNet (Chang et al., 2015) has 51300 3D CAD models in 55 categories, and ModelNet40 (Wu et al., 2015) has 12311 3D CAD models in 40 categories. Recently, a large-scale 3D CAD model dataset, Objaverse (Deitke et al., 2022), consisting of 818k objects and 21k categories, is proposed to enable research in a wide range of areas across computer vision. For the real-scanned 3D object datasets, ScanObjectNN (Uy et al., 2019) is a real-world point cloud object dataset based on scanned indoor scenes, containing around 15k objects in 15 categories. OmniObject3D (Wu et al., 2023b) includes 6k 3D objects in 190 large-vocabulary categories, sharing common classes with popular 2D and 3D datasets. Our method validates that these various 3D object datasets with large vocabulary categories could greatly benefit open-vocabulary 3D object detection.

2.2 OPEN-VOCABULARY OBJECT DETECTION

Open-vocabulary object detection aims at detecting the categories that are not provided bounding box labels during training (Zareian et al., 2021), which first rises in 2D domain due to the large amount of image-text and region-text pairs (Schuhmann et al., 2022; Sharma et al., 2018). Most methods either directly use large-scale image-text pairs (Lin et al., 2023; Zhou et al., 2022a) to provide weak supervision signals when training the detectors or adopt the vision-language models (Radford et al., 2021) pre-trained on large-scale image-text pairs by distillation (Gu et al., 2021; Wu et al., 2023a), fine-tuning (Zhong et al., 2022), or freezing (Kuo et al., 2022). In 3D domain, utilizing the corresponding 2D images of the point cloud scene, recent approaches (Lu et al., 2023; 2022) first use pseudo 3D bounding boxes in training to obtain the localization ability and then connect the point cloud with the image by CLIP (Radford et al., 2021) or image classification dataset (Deng et al., 2009) to empower the 3D detector open-vocabulary recognition ability. Our method directly uses large-scale large-vocabulary 3D object datasets to achieve both open-vocabulary 3D localization and recognition simultaneously in an end-to-end manner, alleviating the need of corresponding 2D images.

2.3 OPEN-VOCABULARY 3D UNDERSTANDING

Previous open-vocabulary 3D understanding mainly focused on 3D recognition or semantic segmentation tasks. Some works (Zhang et al., 2022; Zhu et al., 2022; Huang et al., 2022; Zeng et al., 2023; Xue et al., 2023) explore different strategies to exploit CLIP (Radford et al., 2021) to align 3D object and text for classification. However, these methods can hardly be directly applied to scene-level understanding. Besides, recent works (Peng et al., 2023; Ding et al., 2022) focus on leveraging corresponding 2D posed images and well-established vision-language models to achieve open-vocabulary 3D semantic segmentation. However, it’s hard to obtain the instance 3D bounding box from the point cloud semantic segmentation results. Our method aims to achieve open-vocabulary 3D detection which is an instance-level 3D understanding task.

2.4 3D REFERENTIAL LANGUAGE GROUNDING

Conventional 3D visual grounding methods (Zhao et al., 2021; Achlioptas et al., 2020; Feng et al., 2021; He et al., 2021; Huang et al., 2021; Roh et al., 2022; Yuan et al., 2021) adopt a ‘detect-then-match’ paradigm. These methods first obtain the text features and object proposals by a pre-trained language model and a 3D detector, respectively, then learn to match the object and text features in training and select the best-matched object for each concept in inference. The recent rising one-stage

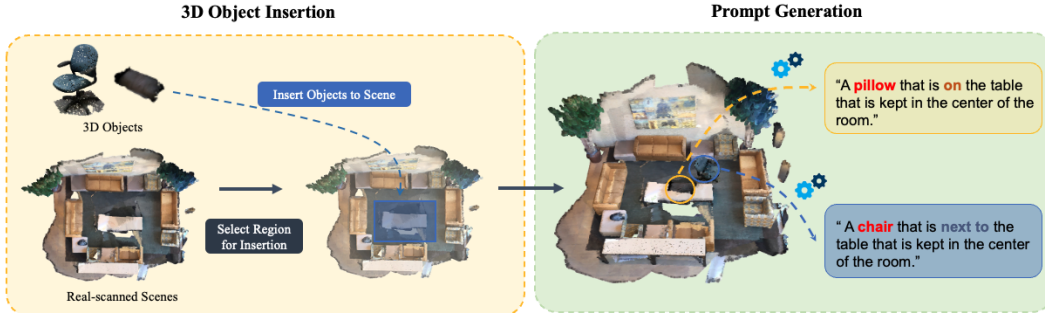


Figure 2: Overall pipeline for Object2Scene. The objects are sampled from 3D object datasets and inserted into the real-scanned scene. Then we generate grounding prompts for the inserted objects.

methods (Jain et al., 2022; Wu et al., 2022; Luo et al., 2022) tend to fuse the text feature into the process of point-cloud feature extraction and detect the text-conditioned object directly, which tends to produce better results. Our proposed L3Det further simplifies the one-stage detector architecture and is generic to language-guided 3D object detection.

3 OBJECT2SCENE

To tackle open-vocabulary 3D object detection with the limited annotations in existing 3D scene datasets, we propose **Object2Scene**. As shown in Figure 2, Object2Scene first inserts 3D objects from large-scale large-vocabulary 3D object datasets (Chang et al., 2015; Uy et al., 2019; Deitke et al., 2022) into 3D scenes to enrich the vocabulary size (Section 3.1), and then generates grounding prompts for the inserted objects (Section 3.2).

3.1 ANCHOR-GUIDED 3D OBJECT INSERTION

The key to empowering the 3D object detector with open-vocabulary abilities is to relate the 3D object representations with large-vocabulary text. Unlike 2D methods that can take advantage of large amounts of image-text pairs, large-scale 3D point-cloud-caption pairs for point cloud scenes are infeasible, while 3D object datasets are more economical and tend to include large vocabulary sizes. Thus, we introduce large-scale and large-vocabulary 3D object datasets into the 3D scenes. However, simple random insertion of objects into the scenes often disrupts the coherence of the scene and makes it hard to generate text descriptions. Since the seen objects annotations are accessible, these objects can act as reference objects (anchors) to guide the object insertion, so we propose a physically reasonable insertion approach: **Anchor-guided 3D Object Insertion** with three steps: Anchor and Object Selection, Object Normalization and Resampling, and Object Placement.

Object and Anchor Selection. We randomly choose one object from the seen objects in the scene as the anchor, and then we randomly sample one object as the target object from the 3D object datasets. The target object comes from a large vocabulary size and may belong to seen or unseen categories except the same category as the anchor.

Object Normalization and Resampling. Due to the different scanning devices and different approaches for data collection and pre-processing, there exists the domain gap of point cloud distributions among different 3D datasets. We predefined a collection of similar objects categories. For the target object, if there exist similar categories in the seen categories, we first normalize the scale of the target object to the average size of the similar category objects and then resample the point cloud to match the average number of points.

Object Placement. In order to place objects in a physically reasonable way, we divide objects into three types, stander, supporter, and supporttee, following Xu et al. (2022). Standeres are objects that can only be supported by the ground and cannot support other objects. Supporteres are objects that can only be supported by the ground and can support other objects. Supporttees are objects that supporteres can support. We place the target in potentially physically valid locations around the anchor. Specifically, a rectangular region centered at the anchor location (x_a, y_a) is determined, and then we compute a z axis height map of the insertion region and iteratively sample centroid

coordinates candidates where the target can be placed. Then we will check whether the placement is physically reasonable according to 1) the categories that the anchor and target belong to (stander, supporter, or supportee), and 2) whether the inserted target would collide with existing objects in the scene.

3.2 OBJECT GROUNDING PROMPT GENERATION

The 3D object insertion approach composes new 3D scenes with original scenes annotated by seen categories and new objects from large vocabulary categories covering seen and unseen categories. A straightforward way of deriving detection annotations is augmenting the existing object detection annotations of the seen classes with the bounding boxes and class labels of the inserted objects from large-vocabulary 3D datasets, and directly training the detector on the augmented 3D detection datasets. However, such naive label assignment mechanism brings up the inconsistent annotation problem mentioned in Section 1. Such inconsistencies may cause ambiguity in annotations and hinder the training of the open-vocabulary 3D detection models in the regular detection training paradigm. Therefore, we propose to generate language grounding prompts to reduce the ambiguity of category-level annotations and to provide clear training guidance for the models.

Similar to SR3D (Achlioptas et al., 2020), we can generate the spatial prompt for the inserted target object according to the following template: $\langle target - class \rangle \langle spatial - relationship \rangle \langle anchor - class \rangle$, e.g. "the table that is next to the plant". The spatial relationship can be categorized into three types: Horizontal Proximity, Vertical Proximity, and Allocentric, according to the location of the anchor and target and the intrinsic self-orientation of the anchor. More details can be found in our appendix. However, the generated simple spatial prompt sometimes may not be strong enough to distinguish the target from other same-category objects in the scene. To further diminish the ambiguity of annotations, we combine the generated spatial utterance and the ground-truth referring expression of the anchor together and generate the **Relative Location Prompt**. For example, if the reference object when inserting the table is a plant with a ground-truth referring expression grounding annotation "a plant that is at the room center", we can generate the prompt for the newly inserted table as "a table that is next to a plant that is at the room center". It is guaranteed that the generated prompt uniquely refers to the table because the original grounding prompt uniquely refers to the plant.

To validate the effectiveness of our proposed Relative Location Prompt, we further propose **Absolute Location Prompt**, a much simpler generated prompt which reduces the prompt ambiguity by specifying the absolute location of the object within the scene for comparison. For example, "a table that is closer to the center/corner of the room". However, such prompts are limited by fewer ways of expression and unclear descriptions which may not be discriminative.

4 OPEN-VOCABULARY 3D OBJECT DETECTION WITH OBJECT2SCENE

In order to train an open-vocabulary 3D object detector with the proposed Object2Scene, we propose a new, simple, but strong baseline that unifies 3D detection and 3D visual grounding, named **L3Det** (Language-grounded 3D object detection). L3Det enables training with both detection prompts and more accurate grounding prompts introduced in Section 3. We leverage the 3D scenes and text prompts generated by Object2Scene for training. To mitigate the domain gap between the feature representations of inserted objects and existing objects in the original scene, we propose a **cross-domain category-level contrastive learning** approach to force source-agnostic generalizable feature representations for the multiple-source 3D objects in the 3D scenes.

4.1 L3DET: LANGAUGE-GROUNDED 3D OBJECT DETECTION

Model Architecture. Our L3Det model follows the generic transformer-based design with the encoder-decoder architecture, as shown in the left side of Figure 3. The input to the model is a point cloud and a text prompt. We extract the point visual tokens $\mathbf{V} \in \mathbb{R}^{n \times d}$ with the PointNet++ encoder and text queries $\mathbf{T} \in \mathbb{R}^{l \times d}$ with the pre-trained RoBERTa text encoder, where $l = 256$ is the maximum length of the text. Following BUTD-DETR (Jain et al., 2022), the top- K highest scoring visual tokens are fed into an MLP to predict the non-parametric object queries, which are updated iteratively through N decoder layers. In each decoder layer, the text queries and non-

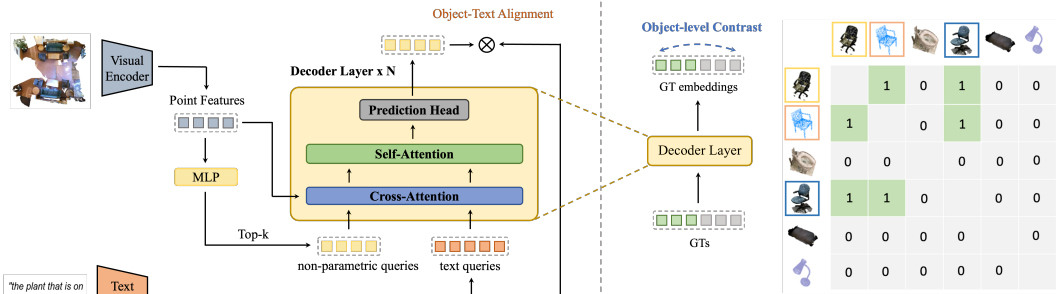


Figure 3: Open-vocabulary 3D object detection with Object2Scene. The figure on the left-hand side shows the model architecture of L3Det. The figure on the right-hand side shows the cross-domain category-level contrastive learning approach. Given 6 objects illustrated in the figure, the contrastive loss brings together (denoted by “1” in the matrix) the features of the three objects belonging to the category “chair”, despite the fact that they are from different source datasets. The object features of different categories are pushed away from each other (denoted by “0” in the matrix).

parametric object queries attend to the point visual features \mathbf{V} with cross-attention to gather the visual information, followed by a self-attention among non-parametric queries and text queries. Finally, the prediction head takes the updated object queries as input and predicts the 3D boxes and object features for aligning the predicted objects with text tokens.

Training Supervision. The overall training supervision is the summation of three loss terms: localization loss \mathcal{L}_{loc} , alignment loss \mathcal{L}_{align} , and our proposed cross-modal category-level contrastive loss \mathcal{L}_{cl} (introduced in Section 4.2). The localization loss \mathcal{L}_{loc} is a combination of L1 and generalized IoU (Rezatofighi et al., 2019) losses between predicted and ground-truth bounding boxes. Following GLIP (Li et al., 2022), the alignment loss measures the alignment between predicted object features and the text queries. Specifically, we compute the object-text alignment scores by $\mathbf{S}_{align} = \mathbf{P}\mathbf{T}^T$, where $\mathbf{P} \in \mathbb{R}^{N \times d}$ is the object features predicted by the prediction head and $\mathbf{T} \in \mathbb{R}^{l \times d}$ is the text queries extracted by the pretrained text encoder. We calculate the target alignment score matrix $\mathbf{S}_{target} \in \{0, 1\}^{N \times M}$ based on the ground-truth alignment between box locations and text query tokens. Binary sigmoid loss (Li et al., 2022) between \mathbf{S}_{align} and \mathbf{S}_{target} is adopted for the alignment loss.

Detection Prompts Supervision. Following BUTD-DETR (Jain et al., 2022), we empower the L3Det general detection ability with detection prompts comprised of a list of object category labels. For the detection prompts, the task is to identify and locate all objects belonging to the category labels mentioned in the prompt, if they are present in the scene.

4.2 CROSS-DOMAIN CATEGORY-LEVEL CONTRASTIVE LEARNING

As demonstrated in Section 3, our Object2Scene approach inserts 3D objects into 3D scenes to generate enriched scenes for training. A consequent problem is the domain gap between the newly inserted objects and existing objects in the original scene. Since the newly inserted objects are from 3D object datasets that have different data distributions from the 3D scene datasets, causing severe misalignment between their 3D feature representations. To mitigate this challenge, we propose a cross-domain category-level contrastive learning approach that leverages contrastive loss on cross-domain objects to learn source-agnostic 3D feature representations. Since the objects we inserted cover both seen and unseen categories, we can construct positive pairs using the seen objects from different datasets. For example, for seen class *desk*, one constructed positive pair could consist of one *desk* from the existing scene and one *desk* from the other 3D object datasets, and the model is trained to minimize the distance between these two same category objects from different datasets. In this way, the model can learn the general representation of the same seen class objects from different datasets, thereby implicitly improving its generalization ability on unseen classes.

As shown in the right side of Figure 3, let f_i denote the object feature for the i -th object in the mini-batch extracted from a decoder layer. In the mini-batch, objects with the same class labels form positive pairs for contrastive learning and objects with different class labels form negative pairs.

The cross-domain category-level contrastive learning loss can be represented as:

$$\mathcal{L}_{cl} = -\frac{1}{N} \sum_{i=1}^N \log \frac{\sum_{i \neq j, y_i = y_j, j=0, \dots, N} \exp(f_i^\top f_j / \tau)}{\sum_{i \neq k, k=0, \dots, N} \exp(f_i^\top f_k / \tau)}, \quad (1)$$

where N is the number of objects in the mini-batch, y_i denotes the class label of the i -th object, and τ is a temperature hyper-parameter. The contrastive loss is also applied to the features of each decoder layer, similar to the detection losses. It is worth noting that the above loss is a generalized contrastive loss that allows multiple positive samples. With the proposed cross-domain category-level contrastive loss, the model is forced to learn generalizable feature representations based on their class labels irrespective of the source dataset of the objects.

5 EXPERIMENT

In this section, we introduce three benchmarks for open-vocabulary 3D object detection, and conduct extensive experiments and analysis to validate the effectiveness of our proposed Object2Scene.

5.1 BENCHMARKS

OV-ScanNet20. Following OV-3DETIC (Lu et al., 2022), we split 20 categories from ScanNet into 10 seen classes (bathtub, fridge, desk, night stand, counter, door, curtain, box, lamp, bag) and 10 unseen classes (toilet, bed, chair, sofa, dresser, table, cabinet, bookshelf, pillow, sink).

OV-SUN RGB-D20. We split 20 categories from SUN RGB-D datasets into 10 seen classes (table, night stand, cabinet, counter, garbage bin, bookshelf, pillow, microwave, sink, and stool) and 10 unseen classes (toilet, bed, chair, bathtub, sofa, dresser, scanner, fridge, lamp, and desk).

OV-ScanNet200. To fully verify the open-vocabulary ability on a larger number of categories, we resort to the large vocabulary of ScanNet200 (Rozenberszki et al., 2022) where the 200 categories are split into head (66 categories), common (68 categories) and tail (66 categories), based on the frequency of number of labeled surface points in the training set. To achieve an open-vocabulary setting, we define the head categories as seen classes, and common and tail categories as unseen classes.

The evaluation metrics for open-vocabulary object detection are Average Precision (AP) and mean Average Precision (mAP) at IoU thresholds of 0.25, denoted as AP_{25} , mAP_{25} , respectively. To test the open-vocabulary abilities, results are tested on the unseen categories.

5.2 IMPLEMENTATION DETAILS

Three commonly-used 3D object datasets are chosen as the data source for Object2Scene: (1) ShapeNet (Chang et al., 2015) with 55 categories and 51300 objects, (2) OmniObject3D (Uy et al., 2019) with 190 categories and 6k objects, and (3) Objaverse (Deitke et al., 2022) with 21k categories and 818k objects. We introduce objects from ShapeNet and OmniObject3D for the OV-ScanNet20 and OV-SUN RGB-D20 benchmark and additionally Objaverse for the OV-ScanNet200 benchmark.

During training, we use the class labels to form the detection prompts. Specifically, OV-ScanNet20 and OV-SUN RGB-D20, we generate the detection prompts by sequencing the 20 class names. For OV-ScanNet200, we randomly sample 20 categories to generate the detection prompts for each training iteration. For Relative Location Prompt generation, and for SUN RGB-D dataset, we generate synthetic referring express generation, we choose ScanRefer (Chen et al., 2020) for ScanNet dataset as referring expression grounding annotations, and for SUN RGB-D dataset, we generate synthetic referring expression grounding annotations following SR3D generation process (Achlioptas et al., 2020).

5.3 MAIN RESULTS

We report our results on three benchmarks and compare them with previous methods on OV-ScanNet20 and OV-SUN RGB-D20 benchmarks. We compare our proposed approach with previous approaches OV-PointCLIP (Zhang et al., 2022), OV-Image2Point (Xu et al., 2021), Detic-

Table 1: Detection results (AP_{25}) on unseen classes of OV-ScanNet20.

| Methods | toilet | bed | chair | sofa | dresser | table | cabinet | bookshelf | pillow | sink | mean |
|------------------------------------|--------------|--------------|--------------|--------------|-------------|--------------|--------------|--------------|--------------|--------------|--------------|
| OV-PointCLIP Zhang et al. (2022) | 6.55 | 2.29 | 6.31 | 3.88 | 0.66 | 7.17 | 0.68 | 2.05 | 0.55 | 0.79 | 3.09 |
| OV-Image2Point Xu et al. (2021) | 0.24 | 0.77 | 0.96 | 1.39 | 0.24 | 2.82 | 0.95 | 0.91 | 0.00 | 0.08 | 0.84 |
| Detic-ModelNet Zhou et al. (2022a) | 4.25 | 0.98 | 4.56 | 1.20 | 0.21 | 3.21 | 0.56 | 1.25 | 0.00 | 0.65 | 1.69 |
| Detic-ImageNet Zhou et al. (2022a) | 0.04 | 0.01 | 0.16 | 0.01 | 0.52 | 1.79 | 0.54 | 0.28 | 0.04 | 0.70 | 0.41 |
| OV-3DETRIC Lu et al. (2022) | 48.99 | 2.63 | 7.27 | 18.64 | 2.77 | 14.34 | 2.35 | 4.54 | 3.93 | 21.08 | 12.65 |
| L3Det | 56.34 | 36.15 | 16.12 | 23.02 | 8.13 | 23.12 | 14.73 | 17.27 | 23.44 | 27.94 | 24.62 |

Table 2: Detection results (AP_{25}) on unseen classes of OV-SUN RGB-D20.

| Methods | toilet | bed | chair | bathtub | sofa | dresser | scanner | fridge | lamp | desk | mean |
|------------------------------------|--------------|--------------|--------------|--------------|--------------|--------------|-------------|--------------|--------------|--------------|--------------|
| OV-PointCLIP Zhang et al. (2022) | 7.90 | 2.84 | 3.28 | 0.14 | 1.18 | 0.39 | 0.14 | 0.98 | 0.31 | 5.46 | 2.26 |
| OV-Image2Point Xu et al. (2021) | 2.14 | 0.09 | 3.25 | 0.01 | 0.15 | 0.55 | 0.04 | 0.27 | 0.02 | 5.48 | 1.20 |
| Detic-ModelNet Zhou et al. (2022a) | 3.56 | 1.25 | 2.98 | 0.02 | 1.02 | 0.42 | 0.03 | 0.63 | 0.12 | 5.13 | 1.52 |
| Detic-ImageNet Zhou et al. (2022a) | 0.01 | 0.02 | 0.19 | 0.00 | 0.00 | 1.19 | 0.23 | 0.19 | 0.00 | 7.23 | 0.91 |
| OV-3DETRIC Lu et al. (2022) | 43.97 | 6.17 | 0.89 | 45.75 | 2.26 | 8.22 | 0.02 | 8.32 | 0.07 | 14.60 | 13.03 |
| L3Det | 34.34 | 54.31 | 29.84 | 51.65 | 34.12 | 17.12 | 5.23 | 13.87 | 11.40 | 15.32 | 25.42 |



Figure 4: Qualitative results for open-vocabulary 3D object detection results. For each scene, the detection prompt is shown under the input point cloud. The colors of bounding boxes correspond to the classes in the prompts.

ModelNet (Zhou et al., 2022a), Detic-ImageNet (Zhou et al., 2022a), and OV-3DETRIC (Lu et al., 2022) introduced in (Lu et al., 2022). The results are presented in Table 1 and Table 2. The results reveal that our Object2Scene, by resorting to the 3D object datasets to enable open-vocabulary 3D detection, outperforms previous state-of-the-art by 12.56% and 23.16% in mAP_{25} on OV-ScanNet20 and OV-SUN RGB-D20, respectively. OV-PointCLIP and Detic-ModelNet obtain open-vocabulary abilities from ModelNet, but both approaches perform poorly due to the large domain gap between the CAD 3D models and point clouds of ScanNet and SUN RGB-D obtained from RGB-D sensors. OV-Image2Point and Detic-ImageNet try to directly transfer the knowledge from image to point cloud which ignores the modality gap between 2D and 3D. Our proposed Object2Scene approach and L3Det with cross-domain category-level contrastive loss alleviate the aforementioned issues of previous approaches and achieve state-of-the-art performance. We also test our approach on OV-ScanNet200 benchmark, and the mAP_{25} on unseen categories is 10.1% for common categories and 3.4% for tail categories. We illustrate the qualitative results on ScanNet dataset in Figure 4.

5.4 ABLATION STUDY

We conduct ablation studies on the OV-ScanNet20 benchmark to justify the contributions of each component and compare various design choices.

Diversity of the inserted 3D objects We investigate whether introducing diverse 3D objects from multiple 3D object datasets helps the model learn better 3D representations for open-vocabulary 3D object detection. For the OV-ScanNet20 benchmark, we experiment with inserting objects from ShapeNet only, from OmniObject3D only, and from both ShapeNet and OmniObject3D, respectively. Evaluation results are shown in Table 3a, where the “overlap mAP_{25} ” refers to the mAP_{25} of categories that can retrieve object instances from both ShapeNet and OmniObject3D datasets, and “ mAP_{25} ” refers to the commonly-defined mAP_{25} averaged over all unseen classes. The ablation study results demonstrate the effectiveness of introducing more diverse objects by leveraging multiple datasets from different sources.

Table 3: Ablation study on 3D object diversity and generated text prompts.
 (a) Ablation study on 3D object diversity. (b) Ablation study on the generated text prompts.

| 3D object dataset | overlap | mAP_{25} | mAP_{25} | Prompt type | mAP_{25} |
|-------------------------|---------|------------|------------|--------------------------|------------|
| ShapeNet | | 7.87 | 11.21 | Detection Prompt | 14.91 |
| OmniObject3D | | 11.31 | 16.92 | Absolute Location Prompt | 17.42 |
| ShapeNet + OmniObject3D | | 15.67 | 24.62 | Relative Location Prompt | 21.31 |

Table 4: Ablation study on object normalization and resampling, data augmentation, and cross-domain object-level contrastive learning.

| Norm, Resample | Agumentation | Contrastive | mAP_{25} |
|----------------|--------------|-------------|------------|
| | | | 2.34 |
| ✓ | | | 6.41 |
| ✓ | ✓ | | 7.34 |
| ✓ | ✓ | ✓ | 11.21 |

Randomness in 3D object placement We explore whether the randomness introduced in 3D object placement is essential for our approach, *i.e.*, what if the location to insert each object for each scene is fixed without any randomness? To avoid the distraction from the randomness of object selection, we fix the selected objects for each scene. For 3D object placement without randomness, we pre-generate the scenes with inserted objects offline before training starts and fix those generated scenes for each epoch. For 3D object placement with randomness, we adopt the same selected 3D objects for insertion but generate the scenes online and introduce randomness in deciding where to place the selected objects. The results show that the randomness in object placement boosts the performance from 18.48% mAP_{25} to 21.31% mAP_{25} , bringing 2.83% mAP_{25} gain.

Language prompts As introduced in Section 3, the language prompts are critical for training the unified 3D detection and grounding model. We design three types of prompts, namely detection prompts, absolute location prompts, and relative location prompts. We compare the effectiveness of those three types of prompts for learning the feature representations for unseen classes. Results shown in Table 3 indicate that the relative location prompts are the most effective language prompts for open-vocabulary 3D detection. This observation aligns with our assumption that the relative location prompts eliminate the inconsistent annotation issue of objects from the unseen categories.

Object normalization and resampling In Section 3.1, we introduce the four steps of inserting a 3D object into a 3D scene, where the second step is normalizing and resampling the 3D object according to the reference point cloud distribution from the 3D scene dataset. This normalization and resampling step is essential for reducing the domain gap between different datasets. As shown in Table 4, the object normalization and resampling increases mAP_{25} from 2.34% to 6.41%.

Data augmentation We apply commonly-used object point cloud augmentation techniques including rotation, point dropping, and jittering for training the object detector. The ablation in Table 4 illustrates that applying the data augmentation further increases mAP_{25} from 6.41% to 7.34%.

Cross-domain category-level contrastive learning We introduce cross-domain category-level contrastive learning to reduce the domain gap between inserted objects from 3D object datasets and existing objects from the original 3D scene datasets. We justify its effectiveness by an ablation study shown in Table 4. In the ablation setup of Table 4, only ShapeNet is regarded as external 3D object dataset to augment the 3D scene dataset. It is shown that the cross-domain category-level contrastive learning method boosts the mAP_{25} of open-vocabulary 3D detection from 7.34% to 11.21%.

6 CONCLUSION

We propose *Object2Scene*, which adopts large-scale large-vocabulary 3D object datasets to enrich the vocabulary of 3D scene datasets for open-vocabulary 3D object detection. We further introduce a unified model, *L3Det*, for 3D detection and grounding, with a cross-domain category-level contrastive loss to bridge the domain gap between inserted objects and original scenes. Extensive experiments and ablations on open-vocabulary 3D detection benchmarks validate the effectiveness of our approach. We believe that our attempt will shed light on future research in open-vocabulary 3D object detection and the broader field of open-world 3D perception.

REFERENCES

- Panos Achlioptas, Ahmed Abdelreheem, Fei Xia, Mohamed Elhoseiny, and Leonidas Guibas. Referit3d: Neural listeners for fine-grained 3d object identification in real-world scenes. In *Computer Vision–ECCV 2020: 16th European Conference, Glasgow, UK, August 23–28, 2020, Proceedings, Part I 16*, pp. 422–440. Springer, 2020.
- Angel X Chang, Thomas Funkhouser, Leonidas Guibas, Pat Hanrahan, Qixing Huang, Zimo Li, Silvio Savarese, Manolis Savva, Shuran Song, Hao Su, et al. Shapenet: An information-rich 3d model repository. *arXiv preprint arXiv:1512.03012*, 2015.
- Dave Zhenyu Chen, Angel X Chang, and Matthias Nießner. Scanrefer: 3d object localization in rgb-d scans using natural language. In *Computer Vision–ECCV 2020: 16th European Conference, Glasgow, UK, August 23–28, 2020, Proceedings, Part XX*, pp. 202–221. Springer, 2020.
- Angela Dai, Angel X Chang, Manolis Savva, Maciej Halber, Thomas Funkhouser, and Matthias Nießner. Scannet: Richly-annotated 3d reconstructions of indoor scenes. In *Proceedings of the IEEE conference on computer vision and pattern recognition*, pp. 5828–5839, 2017.
- Matt Deitke, Dustin Schwenk, Jordi Salvador, Luca Weihs, Oscar Michel, Eli VanderBilt, Ludwig Schmidt, Kiana Ehsani, Aniruddha Kembhavi, and Ali Farhadi. Objaverse: A universe of annotated 3d objects. *arXiv preprint arXiv:2212.08051*, 2022.
- Jia Deng, Wei Dong, Richard Socher, Li-Jia Li, Kai Li, and Li Fei-Fei. Imagenet: A large-scale hierarchical image database. In *CVPR*, 2009.
- Runyu Ding, Jihan Yang, Chuhui Xue, Wenqing Zhang, Song Bai, and Xiaojuan Qi. Pla: Language-driven open-vocabulary 3d scene understanding. *arXiv preprint arXiv:2211.16312*, 2022.
- Mingtao Feng, Zhen Li, Qi Li, Liang Zhang, XiangDong Zhang, Guangming Zhu, Hui Zhang, Yaonan Wang, and Ajmal Mian. Free-form description guided 3d visual graph network for object grounding in point cloud. In *Proceedings of the IEEE/CVF International Conference on Computer Vision*, pp. 3722–3731, 2021.
- Xiuye Gu, Tsung-Yi Lin, Weicheng Kuo, and Yin Cui. Open-vocabulary object detection via vision and language knowledge distillation. In *ICLR*, 2021.
- Dailan He, Yusheng Zhao, Junyu Luo, Tianrui Hui, Shaofei Huang, Aixi Zhang, and Si Liu. Transfer3d: Entity-and-relation aware transformer for fine-grained 3d visual grounding. In *Proceedings of the 29th ACM International Conference on Multimedia*, pp. 2344–2352, 2021.
- Pin-Hao Huang, Han-Hung Lee, Hwann-Tzong Chen, and Tyng-Luh Liu. Text-guided graph neural networks for referring 3d instance segmentation. In *Proceedings of the AAAI Conference on Artificial Intelligence*, volume 35, pp. 1610–1618, 2021.
- Tianyu Huang, Bowen Dong, Yunhan Yang, Xiaoshui Huang, Rynson WH Lau, Wanli Ouyang, and Wangmeng Zuo. Clip2point: Transfer clip to point cloud classification with image-depth pre-training. *arXiv preprint arXiv:2210.01055*, 2022.
- Ayush Jain, Nikolaos Gkanatsios, Ishita Mediratta, and Katerina Fragkiadaki. Bottom up top down detection transformers for language grounding in images and point clouds. In *Computer Vision–ECCV 2022: 17th European Conference, Tel Aviv, Israel, October 23–27, 2022, Proceedings, Part XXXVI*, pp. 417–433. Springer, 2022.
- Weicheng Kuo, Yin Cui, Xiuye Gu, A. J. Piergiovanni, and Anelia Angelova. F-VLM: Open-vocabulary object detection upon frozen vision and language models. *CoRR*, abs/2209.15639, 2022.
- Liunian Harold Li, Pengchuan Zhang, Haotian Zhang, Jianwei Yang, Chunyuan Li, Yiwu Zhong, Lijuan Wang, Lu Yuan, Lei Zhang, Jenq-Neng Hwang, Kai-Wei Chang, and Jianfeng Gao. Grounded language-image pre-training. In *CVPR*, 2022.
- Chuang Lin, Peize Sun, Yi Jiang, Ping Luo, Lizhen Qu, Gholamreza Haffari, Zehuan Yuan, and Jianfei Cai. Learning object-language alignments for open-vocabulary object detection. In *ICLR*, 2023.

-
- Yinhan Liu, Myle Ott, Naman Goyal, Jingfei Du, Mandar Joshi, Danqi Chen, Omer Levy, Mike Lewis, Luke Zettlemoyer, and Veselin Stoyanov. Roberta: A robustly optimized bert pretraining approach. *arXiv preprint arXiv:1907.11692*, 2019.
- Ze Liu, Zheng Zhang, Yue Cao, Han Hu, and Xin Tong. Group-free 3d object detection via transformers. In *Proceedings of the IEEE/CVF International Conference on Computer Vision*, pp. 2949–2958, 2021.
- Yuheng Lu, Chenfeng Xu, Xiaobao Wei, Xiaodong Xie, Masayoshi Tomizuka, Kurt Keutzer, and Shanghang Zhang. Open-vocabulary 3d detection via image-level class and debiased cross-modal contrastive learning. *arXiv preprint arXiv:2207.01987*, 2022.
- Yuheng Lu, Chenfeng Xu, Xiaobao Wei, Xiaodong Xie, Masayoshi Tomizuka, Kurt Keutzer, and Shanghang Zhang. Open-vocabulary point-cloud object detection without 3d annotation. *arXiv preprint arXiv:2304.00788*, 2023.
- Junyu Luo, Jiahui Fu, Xianghao Kong, Chen Gao, Haibing Ren, Hao Shen, Huaxia Xia, and Si Liu. 3d-sps: Single-stage 3d visual grounding via referred point progressive selection. In *Proceedings of the IEEE/CVF Conference on Computer Vision and Pattern Recognition*, pp. 16454–16463, 2022.
- Ishan Misra, Rohit Girdhar, and Armand Joulin. An end-to-end transformer model for 3d object detection. In *Proceedings of the IEEE/CVF International Conference on Computer Vision*, pp. 2906–2917, 2021.
- Songyou Peng, Kyle Genova, Chiyu Jiang, Andrea Tagliasacchi, Marc Pollefeys, Thomas Funkhouser, et al. Openscene: 3d scene understanding with open vocabularies. In *Proceedings of the IEEE/CVF Conference on Computer Vision and Pattern Recognition*, pp. 815–824, 2023.
- Charles Ruizhongtai Qi, Li Yi, Hao Su, and Leonidas J Guibas. Pointnet++: Deep hierarchical feature learning on point sets in a metric space. *Advances in neural information processing systems*, 30, 2017.
- Alec Radford, Jong Wook Kim, Chris Hallacy, Aditya Ramesh, Gabriel Goh, Sandhini Agarwal, Girish Sastry, Amanda Askell, Pamela Mishkin, Jack Clark, et al. Learning transferable visual models from natural language supervision. In *ICML*, 2021.
- Hamid Rezatofighi, Nathan Tsoi, JunYoung Gwak, Amir Sadeghian, Ian Reid, and Silvio Savarese. Generalized intersection over union: A metric and a loss for bounding box regression. In *Proceedings of the IEEE/CVF conference on computer vision and pattern recognition*, pp. 658–666, 2019.
- Tal Ridnik, Emanuel Ben-Baruch, Asaf Noy, and Lihi Zelnik-Manor. Imagenet-21k pretraining for the masses. In *NeurIPS*, 2021.
- Junha Roh, Karthik Desingh, Ali Farhadi, and Dieter Fox. Languagerefer: Spatial-language model for 3d visual grounding. In *Conference on Robot Learning*, pp. 1046–1056. PMLR, 2022.
- David Rozenberszki, Or Litany, and Angela Dai. Language-grounded indoor 3d semantic segmentation in the wild. In *Computer Vision–ECCV 2022: 17th European Conference, Tel Aviv, Israel, October 23–27, 2022, Proceedings, Part XXXIII*, pp. 125–141. Springer, 2022.
- Christoph Schuhmann, Romain Beaumont, Richard Vencu, Cade Gordon, Ross Wightman, Mehdi Cherti, Theo Coombes, Aarush Katta, Clayton Mullis, Mitchell Wortsman, Patrick Schramowski, Srivatsa Kundurthy, Katherine Crowson, Ludwig Schmidt, Robert Kaczmarczyk, and Jenia Jitsev. LAION-5B: An open large-scale dataset for training next generation image-text models. *CoRR*, abs/2210.08402, 2022. doi: 10.48550/arXiv.2210.08402.
- Piyush Sharma, Nan Ding, Sebastian Goodman, and Radu Soricut. Conceptual captions: A cleaned, hypernymed, image alt-text dataset for automatic image captioning. In *ACL*, 2018.

-
- Shaoshuai Shi, Chaoxu Guo, Li Jiang, Zhe Wang, Jianping Shi, Xiaogang Wang, and Hongsheng Li. Pv-rcnn: Point-voxel feature set abstraction for 3d object detection. In *Proceedings of the IEEE/CVF Conference on Computer Vision and Pattern Recognition*, pp. 10529–10538, 2020.
- Mikaela Angelina Uy, Quang-Hieu Pham, Binh-Son Hua, Thanh Nguyen, and Sai-Kit Yeung. Revisiting point cloud classification: A new benchmark dataset and classification model on real-world data. In *Proceedings of the IEEE/CVF international conference on computer vision*, pp. 1588–1597, 2019.
- Size Wu, Wenwei Zhang, Sheng Jin, Wentao Liu, and Chen Change Loy. Aligning bag of regions for open-vocabulary object detection. In *CVPR, 2023a*.
- Tong Wu, Jiarui Zhang, Xiao Fu, Yuxin Wang, Jiawei Ren, Liang Pan, Wayne Wu, Lei Yang, Jiaqi Wang, Chen Qian, et al. Omniobject3d: Large-vocabulary 3d object dataset for realistic perception, reconstruction and generation. *arXiv preprint arXiv:2301.07525*, 2023b.
- Yanmin Wu, Xinhua Cheng, Renrui Zhang, Zesen Cheng, and Jian Zhang. Eda: Explicit text-decoupling and dense alignment for 3d visual and language learning. *arXiv preprint arXiv:2209.14941*, 2022.
- Zhirong Wu, Shuran Song, Aditya Khosla, Fisher Yu, Linguang Zhang, Xiaoou Tang, and Jianxiong Xiao. 3d shapenets: A deep representation for volumetric shapes. In *Proceedings of the IEEE conference on computer vision and pattern recognition*, pp. 1912–1920, 2015.
- Chenfeng Xu, Shijia Yang, Tomer Galanti, Bichen Wu, Xiangyu Yue, Bohan Zhai, Wei Zhan, Peter Vajda, Kurt Keutzer, and Masayoshi Tomizuka. Image2point: 3d point-cloud understanding with 2d image pretrained models. *arXiv preprint arXiv:2106.04180*, 2021.
- Xiuwei Xu, Yifan Wang, Yu Zheng, Yongming Rao, Jie Zhou, and Jiwen Lu. Back to reality: Weakly-supervised 3d object detection with shape-guided label enhancement. In *Proceedings of the IEEE/CVF Conference on Computer Vision and Pattern Recognition*, pp. 8438–8447, 2022.
- Le Xue, Mingfei Gao, Chen Xing, Roberto Martín-Martín, Jiajun Wu, Caiming Xiong, Ran Xu, Juan Carlos Nieves, and Silvio Savarese. Ulip: Learning a unified representation of language, images, and point clouds for 3d understanding. In *Proceedings of the IEEE/CVF Conference on Computer Vision and Pattern Recognition*, pp. 1179–1189, 2023.
- Zhengyuan Yang, Songyang Zhang, Liwei Wang, and Jiebo Luo. Sat: 2d semantics assisted training for 3d visual grounding. In *Proceedings of the IEEE/CVF International Conference on Computer Vision*, pp. 1856–1866, 2021.
- Zhihao Yuan, Xu Yan, Yinghong Liao, Ruimao Zhang, Sheng Wang, Zhen Li, and Shuguang Cui. Instancerefer: Cooperative holistic understanding for visual grounding on point clouds through instance multi-level contextual referring. In *Proceedings of the IEEE/CVF International Conference on Computer Vision*, pp. 1791–1800, 2021.
- Alireza Zareian, Kevin Dela Rosa, Derek Hao Hu, and Shih-Fu Chang. Open-vocabulary object detection using captions. In *CVPR*, 2021.
- Yihan Zeng, Chenhan Jiang, Jiageng Mao, Jianhua Han, Chaoqiang Ye, Qingqiu Huang, Dit-Yan Yeung, Zhen Yang, Xiaodan Liang, and Hang Xu. Clip2: Contrastive language-image-point pretraining from real-world point cloud data. In *Proceedings of the IEEE/CVF Conference on Computer Vision and Pattern Recognition*, pp. 15244–15253, 2023.
- Renrui Zhang, Ziyu Guo, Wei Zhang, Kunchang Li, Xupeng Miao, Bin Cui, Yu Qiao, Peng Gao, and Hongsheng Li. Pointclip: Point cloud understanding by clip. In *Proceedings of the IEEE/CVF Conference on Computer Vision and Pattern Recognition*, pp. 8552–8562, 2022.
- Lichen Zhao, Daigang Cai, Lu Sheng, and Dong Xu. 3dvg-transformer: Relation modeling for visual grounding on point clouds. In *Proceedings of the IEEE/CVF International Conference on Computer Vision*, pp. 2928–2937, 2021.

-
- Yiwu Zhong, Jianwei Yang, Pengchuan Zhang, Chunyuan Li, Noel Codella, Liunian Harold Li, Luowei Zhou, Xiyang Dai, Lu Yuan, Yin Li, et al. RegionCLIP: Region-based language-image pretraining. In *CVPR*, 2022.
- Xingyi Zhou, Rohit Girdhar, Armand Joulin, Phillip Krähenbühl, and Ishan Misra. Detecting twenty-thousand classes using image-level supervision. In *ECCV*, 2022a.
- Zixiang Zhou, Xiangchen Zhao, Yu Wang, Panqu Wang, and Hassan Foroosh. Centerformer: Center-based transformer for 3d object detection. In *Computer Vision—ECCV 2022: 17th European Conference, Tel Aviv, Israel, October 23–27, 2022, Proceedings, Part XXXVIII*, pp. 496–513. Springer, 2022b.
- Xiangyang Zhu, Renrui Zhang, Bowei He, Ziyao Zeng, Shanghang Zhang, and Peng Gao. Pointclip v2: Adapting clip for powerful 3d open-world learning. *arXiv preprint arXiv:2211.11682*, 2022.

A EXPERIMENT DETAILS

This section provides more implementation details of the proposed Object2Scene approach and L3Det model.

Prompt Generation for Object2Scene Here we provide detailed information for the grounding prompt generation process introduced in Section 3.2. Following SR3D, we generate the spatial prompt for the inserted target object using the following template: $\langle target - class \rangle \langle spatial - relationship \rangle \langle anchor - class \rangle$. Since the target and anchor classes are determined during 3D object insertion, we need to describe the spatial relationship according to their relative locations. we divide the spatial object-to-object relations into three categories:

1. **Vertical Proximity:** It indicates the target is *on* the anchor object.
2. **Horizontal Proximity:** This indicates the target is around the anchor object and can be represented by words like: *next to* or *close to*.
3. **Allocentric:** Allocentric relations are actually based on Horizontal Proximity, which encodes information about the location of the target with respect to the self-orientation of the anchor, which can be represented by words like: *left, right, front, back*.

Once we obtain the generated spatial prompt such as *"the table that is next to the bar stool."*, given a text sentence of anchor object *"it is a wood bar stool. The stool is in the kitchen at the bar. It is the very first stool at the bar."* in ScanRefer (Chen et al., 2020), we utilize the off-the-shelf tool to decouple the text and obtain the main object, auxiliary object, attributes, pronoun, and relationship of the sentence as shown in Figure 5, following EDA (Wu et al., 2022). Then we replace the main object in the sentence with the inserted target object and the original main object becomes the auxiliary object. Combining the spatial prompt, the generated grounding prompt could be *"it is a table next to a wood bar stool. The stool is in the kitchen at the bar. The stool is the very first stool at the bar."*

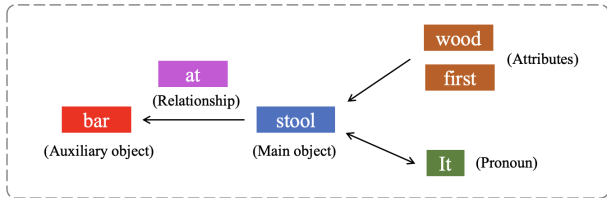


Figure 5: Sentence decoupling illustration.

Details of the model architecture of L3Det In our proposed model L3Det, the point cloud feature tokens $\mathbf{V} \in \mathbb{R}^{n \times d}$ are extracted by PointNet++ (Qi et al., 2017) encoder pre-trained on ScanNet (Dai et al., 2017) seen classes, where $n = 1024$ denotes the number of input points. The text query tokens $\mathbf{T} \in \mathbb{R}^{l \times d}$ are extracted by the pre-trained RoBERTa (Liu et al., 2019) text encoder, where $l = 256$ is the maximum length of the text. The non-parametric queries are predicted with an MLP from the 256 visual tokens with the highest scores. Besides, the number of layers in the decoder is set to $N_E = 6$. The decoder predicts object features $\mathbf{O} \in \mathbb{R}^{k \times d}$, where $k = 256$ is the number of candidate objects, and $d = 288$ is the feature dimension.

Performance in the process of BUTD-DETR simplification to L3Det Table 7 shows the changes in the visual grounding performance from top to bottom during the process of simplifying BUTD-DETR to our L3Det. From the results, it can be seen that by directly inputting text tokens and object queries parallelly into the decoder, it can compensate for the performance drop caused by abandoning the cross-encoder and even achieve better performance ($51.0 \rightarrow 47.2 \rightarrow 51.3$). Besides, using alignment loss following GLIP can further improve the model’s performance to 52.8 (> 52.2 , the performance of BUTD-DETR) while not using box stream compared with BUTD-DETR.

Comparison with existing detection methods for L3Det To demonstrate our L3Det’s strong detection capability, we directly train L3Det on ScanNet 18 classes using the 18 categories combination detection prompt, and the experiments in Table 6 show L3Det achieves higher detection performance.

Table 5: Performance change in the architecture modification from BUTD-DETR to L3Det.

| Method | Accuracy |
|---|----------|
| BUTD-DETR | 52.2 |
| + remove box stream | 51.0 |
| + with concatenated Visual and Language Streams | 50.1 |
| + remove cross-encoder | 47.2 |
| + replace with our L3Det decoder (using parallel text and object query) | 51.3 |
| + replace with GLIP alignment loss (Our L3Det) | 52.8 |

Table 6: 18 class 3D object detection results on ScanNetV2.

| Method | mAP_{50} |
|-------------|------------|
| 3DETR | 44.6 |
| GroupFree3D | 48.9 |
| L3Det | 50.1 |

Combining Object2Scene with existing methods Here we attempt to use Object2Scene to enable the close-set 3D object detector to obtain open-vocabulary detection capability. Since both GroupFree3D and 3DETR are close-set 3D object detectors and do not possess the text input capability, we modified their class prediction to 20 classes, which cover all the categories in OV-ScanNet20 benchmark, but only seen annotations (10 classes) are used for training in the actual training process. Then we introduce unseen objects using Object2Scene to expand the training dataset. Results on OV-ScanNet20 in Table 7 show our Object2Scene is general, and L3Det is also better than GroupFree3D and 3DETR due to the text prompt input ability and architecture advantages.

Table 7: Detection results on unseen classes of OV-ScanNet20.

| Method | mAP_{25} |
|----------------------------|------------|
| 3DETR | 1.31 |
| GroupFree3D | 0.53 |
| 3DETR + Object2Scene | 14.23 |
| GroupFree3D + Object2Scene | 15.16 |
| L3Det + Object2Scene | 23.98 |

Alignment Matrix Generation for L3Det In the second paragraph of Section 4.1 of the main paper, we introduce the training supervision for L3Det, where calculating the alignment loss requires a target alignment score matrix $\mathbf{S}_{target} \in \{0, 1\}^{N \times M}$. The key to generating the target alignment score matrix is the fine-level alignment between the text tokens and 3D boxes which is typically not provided in most of visual grounding datasets including ScanRefer (Chen et al., 2020). We use the off-the-shelf tool following EDA (Wu et al., 2022) to parse the text description, generate the grammatical dependency trees, and obtain the position label. For example, given a sentence "It is a white table. It is next to a backboard" consisting of multiple objects, the main object in this sentence is "table" and the corresponding position label is "0000100...".

Training Details The code is implemented based on PyTorch. Our model is trained on two NVIDIA A100 GPUs with a batch size of 24. We freeze the pretrained text encoder and use a learning rate of 1×10^{-3} for the visual encoder and a learning rate of 1×10^{-4} for all other layers in the network. It takes around 25 minutes to train an epoch, and our model is trained for 120 epochs. The best model is selected based on the performance of the validation set.

B VISUAL GROUNDING RESULTS

Our proposed L3Det model unifies the 3D object grounding and detection with the same framework, and we report the language-based 3D grounding performance trained on ScanRefer (Chen et al., 2020) in Table 8. Compared with previous works such as BUTD-DETR (Jain et al., 2022), our proposed L3Det achieves better grounding results with a simpler model architecture. We hope our proposed L3Det will serve as a new 3D grounding and detection baseline for its simple, effective, and unified model architecture.

Table 8: Performance comparisons on language grounding on ScanRefer (Chen et al., 2020)

| Method | Unique@0.25 | Unique@0.5 | Multi@0.25 | Multi@0.5 | Overall@0.25 | Overall@0.5 |
|--|-------------|-------------|-------------|-------------|--------------|-------------|
| ReferIt3DNet (Achlioptas et al., 2020) | 53.8 | 37.5 | 21.0 | 12.8 | 26.4 | 16.9 |
| ScanRefer (Chen et al., 2020) | 63.0 | 40.0 | 28.9 | 18.2 | 35.5 | 22.4 |
| TGNN (Huang et al., 2021) | 68.6 | 56.8 | 29.8 | 23.2 | 37.4 | 29.7 |
| InstanceRefer (Yuan et al., 2021) | 77.5 | 66.8 | 31.3 | 24.8 | 40.2 | 32.9 |
| FFL-3DOG (Feng et al., 2021) | 78.8 | 67.9 | 35.2 | 25.7 | 41.3 | 34.0 |
| 3DVG-Transformer (Zhao et al., 2021) | 77.2 | 58.5 | 38.4 | 28.7 | 45.9 | 34.5 |
| SAT-2D (Yang et al., 2021) | - | - | - | - | 44.5 | 30.1 |
| BUTD-DETR (Jain et al., 2022) | 84.2 | 66.3 | 46.6 | 35.1 | 52.2 | 39.8 |
| L3Det | 84.8 | 67.1 | 47.1 | 35.9 | 52.8 | 40.2 |

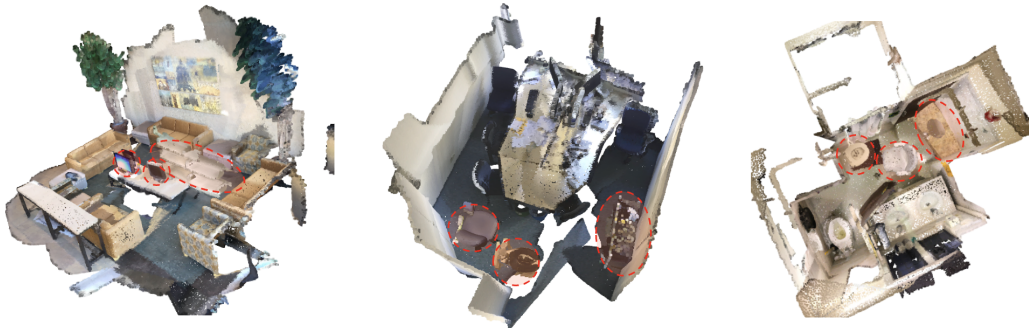


Figure 6: Sample scenes generated by Object2Scene. The objects surrounded by the red circle in the figure are sampled from 3D object datasets and inserted into the real-scanned scene.

C QUALITATIVE ANALYSIS

In this section, we illustrate more scenes generated by our Object2Scene approach in Figure 6 and more visualization results in Figure 7. Figure 6 shows several scenes generated by Object2Scene, where the 3D objects are inserted into the real-scanned scenes in a reasonable manner. As illustrated in Figure 7, L3Det can locate all objects belonging to the category described in the input text prompt covering various object sizes. Nevertheless, we find that our model may sometimes incorrectly detect the objects (illustrated in the top middle sub-figure in Figure 7) or miss the objects. For example, if the chairs are tucked under the table, the actual point cloud distribution of the chairs and the point cloud distribution of chairs we insert into by Object2Scene are often very different, making it difficult to detect. Those failure cases might be due to the distribution misalignment between the scanned point cloud in the scene and the point cloud of the inserted objects from other datasets. We leave this issue for future work.

Table 9: Ablation Study.

(a) Performance of different training epochs when 40% of the 3D objects from the 3D object dataset are used for training.

| Training Epochs | mAP_{25} |
|-----------------|------------|
| 30 | 11.87 |
| 45 | 15.43 |
| 60 | 18.99 |
| 100 | 20.62 |
| 120 | 21.31 |

(b) Performance of different data ratio used in Object2Scene with 120 training epochs. Data ratio refers to the ratio of objects from the 3D object dataset that are used for training. It reflects the diversity of 3D objects that are inserted to the scenes.

| Data Ratio | mAP_{25} |
|------------|------------|
| 40% | 12.56 |
| 80% | 18.11 |
| 100% | 21.31 |

D ABLATION STUDY

In this section, we provide more ablation studies on how to use the data generated by Object2Scene for training. During training, the Object2Scene approach generates augmented scenes online, *i.e.*, the inserted objects and locations to insert objects are sampled at each iteration. We investigate two factors: 1) the number of training epochs, and 2) the diversity of inserted objects, *i.e.*, the ratio of

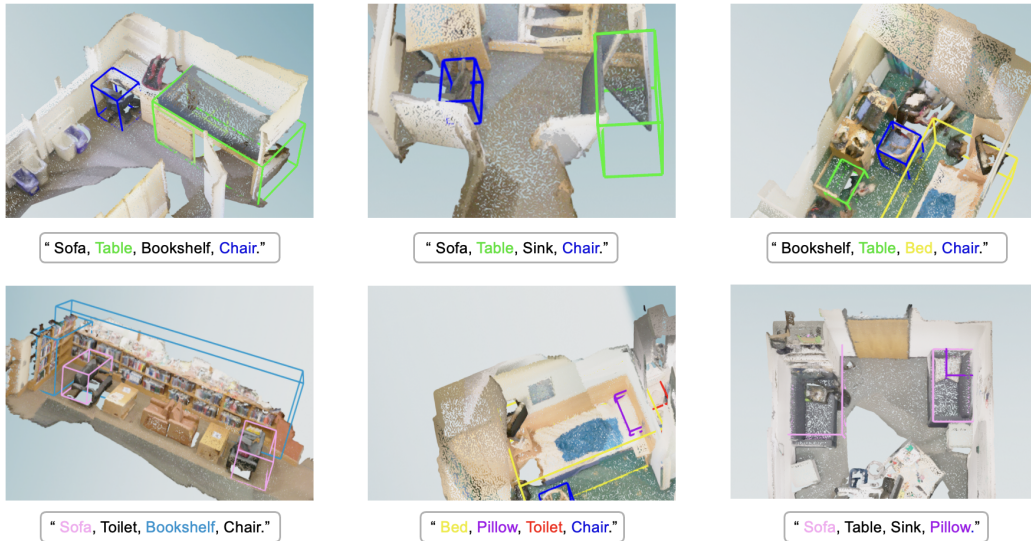


Figure 7: Qualitative results for open-vocabulary 3D object detection results. For each scene, the detection prompt is shown under the input point cloud. The colors of bounding boxes correspond to the classes in the prompts.

data from the 3D object dataset that is used for training. Table 9a demonstrates that more training epochs lead to better performance. Table 9b indicates that increasing the diversity of inserted 3D objects improves the performance.

E TRANSFERABILITY TO NEW DATASETS

We explore the transferability of our 3D detectors by evaluating the cross-dataset transfer performances between OV-ScanNet20 and OV-SUN RGB-D20. The transferability of our 3D detector mainly comes from the pretrained text encoder and the robust and transferable 3D feature representations trained with objects from multiple source datasets using the cross-domain category-level contrastive loss. The object detector trained on OV-ScanNet20 achieves an mAP_{25} of 16.34% when tested on OV-SUN RGB-D20 dataset, and the object detector trained on OV-SUN RGB-D20 achieves an mAP_{25} of 17.11% when tested on OV-ScanNet20, demonstrating the transferability of the object detectors trained with Object2Scene.